Journal of
Orthopaedic
Research®

Intraoperative assembly of anatomical shoulder prosthesis frequently results in malalignment of the modular taper junction

Maria Herbster[1] 🔘 | Alexander Berth[2] | Nicole Märtens[2] | Marcel Robra[2] | Florian Welzel[3] | Frank Dallmann[4] | Christoph H. Lohmann[2] | Thorsten Halle[1] | Jessica Bertrand[2] | Joachim Döring[2]

[1]Institute of Materials and Joining Technology, Otto-von-Guericke University, Magdeburg, Germany

[2]Department of Orthopaedic Surgery, Otto-von-Guericke University, Magdeburg, Germany

[3]GFE—Gesellschaft für Fertigungstechnik und Entwicklung Schmalkalden e.V., Schmalkalden, Germany

[4]Mathys Ltd., Bettlach, Switzerland

Correspondence
Maria Herbster, Institute of Materials and Joining Technology, Otto-von-Guericke University, Universitätsplatz 2, 39106 Magdeburg, Germany.
Email: maria.herbster@ovgu.de

Abstract

Anatomical shoulder arthroplasties (ASA) may fail because of micromotion at the modular taper junction causing wear due to fretting. Sufficient taper strength can reduce micromotion and potential reasons for failure. However, there are no normative standards for a safe assembly process performed intraoperatively by the surgeon. The purpose of this study is to determine the effect of common intraoperative assembly strategies and to identify critical influencing factors on taper stability. ASA with standard and stemless humeral component in combination with concentric Al_2O_3 heads and eccentric CoCr28Mo6 alloyed humeral heads were tested. Taper angles and surface roughness were determined. Force magnitudes and impact directions were recorded using a sensorized head impactor and a three-dimensional force measuring platform. Subsequently, the axial pull-off forces were measured and taper engagement areas were macroscopically evaluated. In comparison to standard stem tapers that were impacted with an assembly device, stemless tapers were impacted into the artificial bone with significantly lower forces. Taper strength correlates to maximum impact force and was higher for CoCr28Mo6 heads with a mean pull-off ratio of 0.56 than for Al_2O_3 heads with 0.37. Interestingly, all tapers showed an asymmetric clamping behavior, due to tilting during impaction. This is caused by the variation of the resulting force vector and further promoted by humeral head eccentricity. Assembly technique markedly influences the force magnitude, impact direction, impulse, and consequently taper strength. The resulting force vector and head eccentricity were identified as potential risk factors for taper malalignment.

KEYWORDS
assembly force, impact direction, modularity, shoulder arthroplasty, taper strength

1 | INTRODUCTION

Anatomical shoulder arthroplasties (ASA) show good outcomes for the treatment of glenohumeral joint osteoarthritis.[1,2] They aim at the restoration of the natural kinematics of the shoulder joint and to improve the patient's quality of life.[3] The affected joint is replaced by insertion of a humeral stem and a connected head into the humeral bone (hemiarthroplasty) or with an additional glenoid component (total arthroplasty). The bone of the proximal humerus exhibits a large variability of geometric dimensions with respect to inclination, retroversion, and/or medial-dorsal offsets.[4,5] To allow an ideal reconstruction of the anatomical geometry and the center of rotation, a variety of implant designs and component sizes as well as modularity for ASA are offered by different manufactures.

Over the past decades, short-stemmed and stemless implants were developed to avoid possible problems and risks of conventional implants. The benefits of this design are humeral bone preservation, reduced risk of periprosthetic fracture, and less complex revision surgery.[6,7] Independent of the stem design, a modular taper system connects the humeral head onto the stem. This modularity allows an intraoperative adaptation of the optimal anatomical fit, a combination of different materials and component sizes as well as an easier component removal during revision surgery.[8] Third- and fourth-generation shoulder prostheses are modular and adaptable to enable a variable three-dimensional (3D) adjustment of inclination and offset in the mediolateral direction.[9] For this purpose, different system designs are available, including eccentric displacement systems[6] or double excenter mechanisms for both the stem and the head taper.[10,11]

Besides the advantages that are associated with modularity, recent studies showed that it bears the risk of implant failures due to corrosion and fretting at the modular taper junction.[12–14] This process, known as mechanically assisted crevice corrosion in total hip arthroplasty, releases metal ions, corrosion products, and wear debris that can elicit adverse local tissue reactions.[14] Retrieval studies demonstrated that taper corrosion can also occur in less weight-bearing anatomical shoulder endoprostheses.[15–17] Micromotion at the modular taper junction initiates fretting corrosion and consequently metal ion and wear release.[18] The process of fretting can already start with the intraoperative impaction of the taper components since it determines taper engagement and taper stability. However, driving factors that cause poor taper strength, such as taper geometry and topography, impaction direction, and force, are not well studied for ASA.

In this regard, the design features of the taper components affect the contact behavior. Consequently, resulting taper clearance should be minimized for a stable taper lock and to prevent component canting.[19,20] Tilting prevents a stable load transfer as envisaged by a congruent engagement.[21] It results in a decreased contact area and generates high-stress foci that cause local wear generation and an increased fretting motion, as demonstrated by Buente et al.[21] on retrieved tapers.

In addition, the impact direction influences the tapered engagement and is recommended to be in axial alignment with the longitudinal axis of the taper junction.[22] Frisch et al.[23,24] showed that off-axis impaction reduces significantly the stability of the modular interface. However, the assembly procedure might restrict the impaction direction and force applied as reported by Nambu et al.[25] For total hip arthroplasty, there is evidence that the magnitude of impact force is a critical factor determining taper strength and subsequent occurrence of micromotion, corrosion, and fretting.[26–28] This emphasized the relevance of the assembly procedure of modular components during surgery. Accordingly, an impaction force of at least 4 kN has been suggested for a sufficient taper fixation for hip implants.[29] There are no standards or recommendations for a secure assembly technique or required impact force of anatomical shoulder endoprostheses. Manufactures provide a polymer impactor with a concave contour to impact the humeral head onto the stem taper during surgery. The assembly procedure can either be performed using an external fixation device or directly onto the humerus bone with the preimpacted stem. The applied ASA impaction forces by the surgeon are yet unknown.

The aim of this study is to determine the impact forces and resulting force vectors of two assembly techniques applied by a surgeon during implantation of shoulder arthroplasties. Therefore, we investigated two common assembly processes for standard stems ($n = 6$) and stemless components ($n = 3$) using an assembly device and direct bone impaction. The taper strengths were then determined by pull-off tests.

2 | MATERIALS AND METHODS

2.1 | Implant characteristics

Two anatomical shoulder implants with a standard stem and a stemless humeral component were investigated (Mathys Ltd.).

Six cemented Affinis stems of titanium base alloy (TiAl6V4) of the size 9, referred to as "standard stems," and three cementless Affinis stemless shoulder prostheses of TiAl6V4 alloy of the size 1, specified as "stemless," were used. Whereas the standard stem surface is shot-peened, the stemless surface is titanium plasma-sprayed and coated with calcium phosphate. All heads had a diameter of 43 mm and a head height of 15 mm. Six ceramic heads fabricated from alumina ceramic (Al_2O_3 Bionit 43/15/2) with a concentric bore taper and three heads made from a cobalt–chromium alloy (CoCr28Mo6 43/15/2) with an eccentric bore taper (offset of 3 mm) were tested (Figure 1). All tested stem tapers had an identical cone design and taper specification.

Before testing, all taper surfaces were scanned pointwise with a Leitz PMM 866 coordinate measuring machine (Hexagon Metrology GmbH) with an LSPX5 probe head. Diameters at five z-levels were measured with 36 scan points and the entity of points mathematically linked via the Gauss method determined the taper angle.

Tactile surface roughness measurements of each taper sample were performed with the measuring device Form Talysurf PGI DIA Testor 7521 (Taylor Hobson Precision). According to DIN EN ISO, 4288:1998 cutoff wavelengths and measuring distances were specified with a 0.8 mm Gaussian filter and 5 × 0.8 mm for the head tapers and a 2.5 mm Gaussian filter on 5 × 2.5 mm for the stem
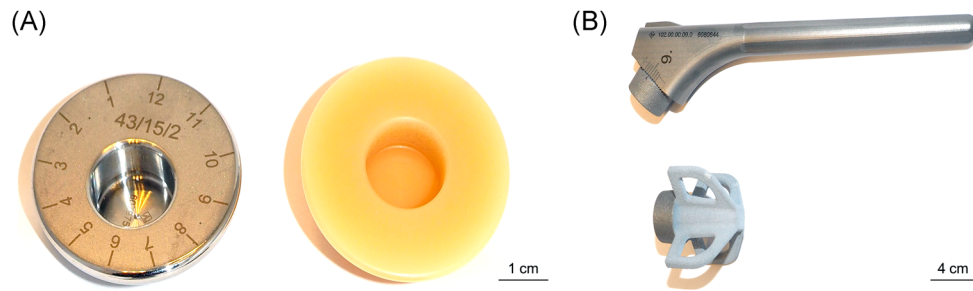
FIGURE 1 Photographs of the tested anatomical shoulder prostheses. (A) Humeral head of CoCr28Mo6 alloy (left) with an eccentric taper and ceramic humeral head of Al_2O_3 (right) with a concentric taper. (B) Affinis standard stem of TiAl6V4 alloy with a modular cone (top) and Affinis stemless component of TiAl6V4 with titanium plasma-sprayed and calcium phosphate coating and fins (bottom) [Color figure can be viewed at wileyonlinelibrary.com]

tapers. All samples were measured at three different locations with a radial distance of 45°. The arithmetic average roughness (R_a), the average maximum profile height (R_z), and the core groove depth (R_k DIN EN ISO 13565-2) were determined.

In addition, 3D topography images were obtained with a confocal microscope (µsurf expert; NanoFocus AG). The measuring field of 1.57 × 1.57 mm was acquired with a ×10 magnification objective and a vertical resolution of 20 nm.

2.2 | Impaction procedures

For standard stem endoprostheses, the assembly device was placed on a vibration-damping mat of rubber to reduce the vibrations on the underlying force measuring platform. Each stem was tightened into the device ensuring a horizontal orientation of the plane taper surface (Figure 2A). The modular stem cone was placed on the determined

position of zero offsets in the medial-lateral direction and tightened to the position by a screw connection with a fixed torque of 12.5 N·m. The humeral head was then placed onto the stem cone without any axial force. For the eccentric CoCr28Mo6 heads, position 12 of zero anterior–posterior offset was chosen. For the investigation, a sensorized (PACEline CLP/62 kN; HBM GmbH) head impactor made of polyoxymethylene was used (Figure 2B). The force measuring platform consisted of a multicomponent dynamometer (type 9255C; Kistler Instrumente AG) with a laboratory charge amplifier (type 5011B) that operated in the measuring field of 0–10,000 N (1000 N/V) with a low-pass filter at 30 kHz. The transformed signals were measured with a sampling rate of 50 kHz by the NI USB-4431 box (National Instruments) and recorded by the software LabView (National Instruments). The surgeon applied typical strokes with a surgical hammer of 500 g with the right arm.

The surgical implantation procedure intends to impact the stemless component with the upper fin surfaces parallel to the resection plane of
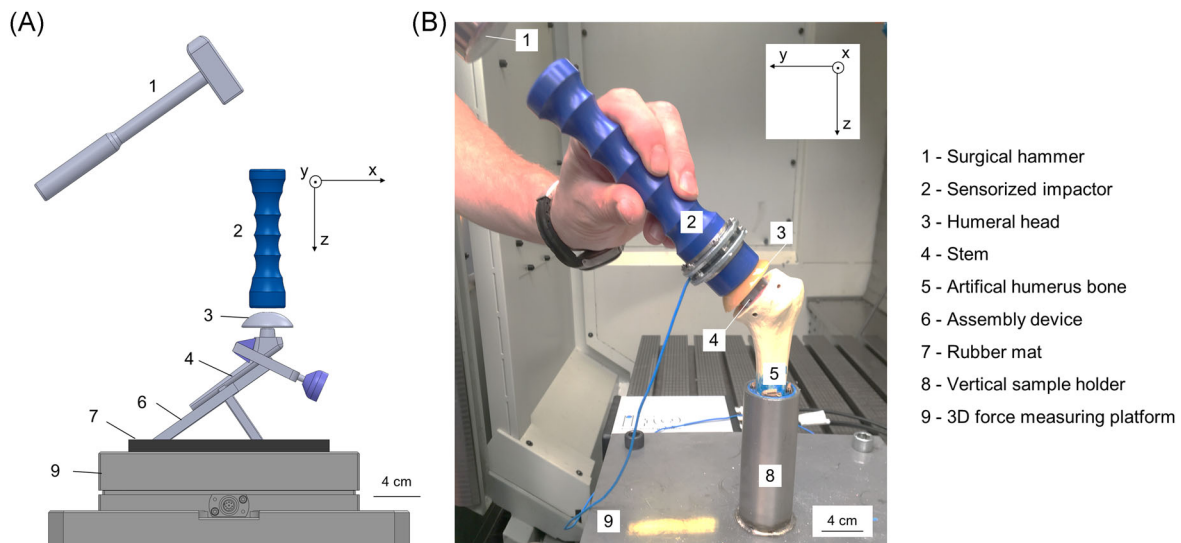

FIGURE 2 Experimental set-up for impaction tests with the defined three-dimensional (3D) coordinate system. (A) Schematic image of the assembly of the humeral head on standard stem using an assembly device. (B) Photograph of a manual impaction of a stemless prosthesis with a ceramic head into the artificial bone using a sensorized impactor. 1—Surgical hammer; 2—sensorized impactor; 3—humeral head; 4—stem; 5—artificial humerus bones; 6—assembly device; 7—rubber mat; 8—vertical sample holder; 9—3D force measuring platform [Color figure can be viewed at wileyonlinelibrary.com]

the humerus.[30] Three artificial humerus bones (medium size, left side, No. 1013, Sawbones Corp.) with cancellous inner material (cellular rigid polyurethane foam 12.5 pcf, density 0.28 g/cm^2) and a solid cortical shell (solid polyurethane 17 pcf, density 1.64 g/cm^2) were prepared using standard surgical tools. After preimpaction, the humeri were positioned and fixed in a vertical sample holder using epoxy resin. The stemless components were preimpacted with the positioner tool until the fins had at least 2 mm of height above the resection plane. The cones were cleaned and dried before the ceramic heads were first mounted by a compressive hand movement. Then, the sensorized hand impactor was applied to impact the prosthesis until the head had an even level with the resection plane.

The angular deviation was calculated as the angle between the maximum resulting force vector, detected in the measuring platform, to the ideal impaction direction which is perpendicular to the frontal plane of the taper. The ideal impaction directions for standard (st) and stemless tapers (sl) are defined as the following unit vectors ($\|u\|=1$):

$$\vec{u}_{st} = \begin{bmatrix} 0 \\ 0 \\ 1 \end{bmatrix}, \tag{1A}$$

$$\vec{u}_{sl} = \begin{bmatrix} 0 \\ \frac{1}{\sqrt{2}} \\ \frac{1}{\sqrt{2}} \end{bmatrix}. \tag{1B}$$

The angular misfit ($\propto$) was calculated using the following equation:

$$\propto_{st} = \cos^{-1}\left(\frac{\vec{u}_{st} \cdot \vec{F}_{res}}{|\vec{u}_{st}| \cdot |\vec{F}_{res}|} \right), \tag{2A}$$

$$\propto_{sl} = \cos^{-1}\left(\frac{\vec{u}_{sl} \cdot \vec{F}_{res}}{|\vec{u}_{sl}| \cdot |\vec{F}_{res}|} \right). \tag{2B}$$

2.3 | Pull-off test

Taper fixation strength was determined in pull-off tests according to ASTM F2009.[31] Before testing, the stems joined with heads were shortened manually with a cut-off grinding machine. Therefore, the standard stem was cut to a length of 40 mm, and all fins of the short

stems were removed as shown in Figure 3. The shortened components were positioned in a sample holder and then were placed into a servo-hydraulic testing machine (Type HBT 100; Zwick Roell GmbH & Co. KG). A linear axial displacement rate of 0.05 mm/s disassembled the taper junction. The control cube servo controller and Cubus testing software recorded continuously the distance traveled and the force applied over time.

2.4 | Evaluation of taper engagement

Taper engagement areas were evaluated with regard to four different radial sectors with 45° offset (shown in Figure 3A). They are referred to as anterior (head position 3), lateral (12), posterior (9), and medial taper area (6).[4] Therefore, the components were photographed and inspected using a stereomicroscope.

2.5 | Statistical analysis

The descriptive data are mean ± standard deviation. Differences between study groups were compared using the one-way analysis of variance with a Bonferroni post hoc test.[32] Level of significance was set at *$p < 0.05$ for all statistical tests. The statistical analysis was performed using Origin software 2018 (OriginLab Corporation).

3 | RESULTS

3.1 | Taper geometry and roughness

Before testing, the initial taper angles and roughness were measured. The mean values of the head and stem taper angles are shown in Figure 4A. A significant difference ($p = 0.002$) was present between the CoCr28Mo6 alloy heads (mean angle of 5.77° ± 0.006°) in comparison to the Al$_2$O$_3$ head tapers (mean angle of 5.786° ± 0.007°).

(A)　　　　　　　(B)　　　　　　　(C)
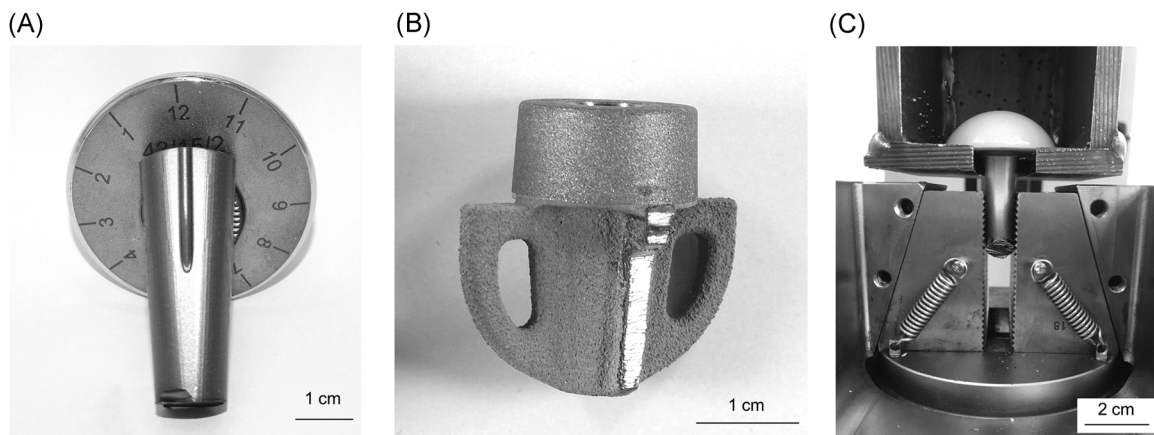
1 cm　　　　　　1 cm　　　　　　2 cm

FIGURE 3 Prepared samples and experimental setup for pull-off tests. (A) Prepared standard stem with assembled humeral head. (B) Prepared stemless component with sawn-off fins. (C) Pull-off device according to ASTM F2009 placed inside a servo-hydraulic testing machine that disassembles a ceramic humeral head from a standard stem
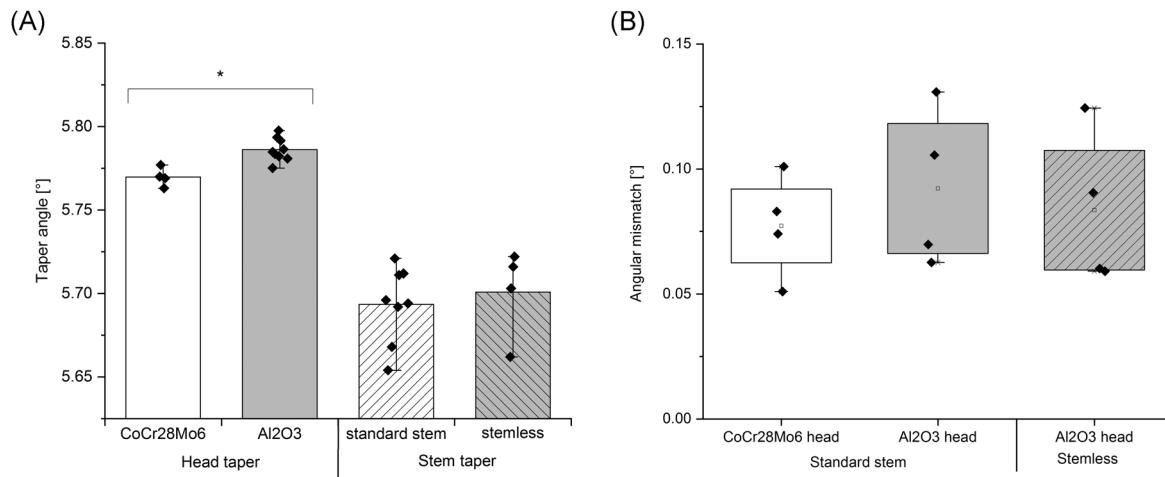
FIGURE 4 Geometric parameters of the investigated stem and head tapers. (A) Taper angles of head and stem tapers according to material and stem design. (B) An angular mismatch between head and stem taper of the assembled taper combinations according to material and stem design (mean ± standard deviation, one-way analysis of variance with Bonferroni post hoc test, in (A) head taper angles *$p = 0.002$, stem taper angles $p = 0.634$)

No difference in mean taper angles was observed between standard and stemless tapers for the different stem designs. Both taper types exhibited similar mean taper angles with 5.69° ± 0.023° and 5.7° ± 0.027°, respectively. In comparison to the head taper angle with an angular variation of 0.02°, the stem taper angles had a greater variation of 0.07° (range from the minimal angle of 5.65° to maximum of 5.72°).

The resulting angular mismatch (known as taper clearance) for the assembled head to stem tapers is presented in Figure 4B. All tested samples exhibited a positive taper clearance in the range from 0.05° to 0.13°, which would result in a deeper taper lock up (proximal direction) between the stem and head taper at axial alignment. Ceramic tapers showed a slightly higher angular mismatch than CoCr28Mo6 humeral head junctions, based on the higher variation of taper angle for the ceramic bore tapers. This difference was not significant between the investigated study groups.

The topography of the new tapers is illustrated by confocal microscopic images and exemplary tactile roughness profiles in Figure 5A–C. Different surface finishes were present on the investigated tapers. CoCr28Mo6 alloy head tapers exhibited periodic machining marks due to a turning process whereas the Al_2O_3 bore tapers had an aperiodic roughness profile based on a grinding process. TiAl6V4 alloy stem tapers also exhibited an aperiodic surface finish due to a final corundum blasting.

The corresponding roughness parameters R_a, R_k, and R_z are shown in Figure 5D. For the head tapers, the mean R_a values varied between 0.45 and 0.77 μm for CoCr28Mo6 and Al_2O_3 head tapers. Regarding the roughness height R_z, Al_2O_3 heads exhibited a doubling of the profile height with 5.49 μm in comparison to CoCr28Mo6 heads with a mean value of 2.03 μm ($p = 0.013$). This significant difference can also be seen in the exemplary roughness profiles (Figure 5A,B). In comparison to the head tapers, the stem tapers exhibited five times higher mean R_a value of 3.5 μm. This

indicates that the head tapers are smoother than the corundum blasted stem tapers. The R_k and R_z values verify the difference between the head and the stem tapers regarding the surface roughness. The mean R_z value for standard and stemless components of 28.6 and 26.3 μm, respectively, exceeded the R_z values of the head tapers by a factor of minimum 5.

3.2 | Impact force magnitude and load–time history

In the scope of impaction tests, two different assembly techniques were performed. First, standard stems were assembled using an assembly device provided by the manufacturer. Then concentric Al_2O_3 humeral heads were impacted to the stemless components that were preimpacted into the artificial humeral bone.

In Figure 6, the load–time curves and magnitudes of the impaction forces measured in the sensorized impactor are illustrated. The joining process of all standard stem prostheses was performed with two strokes and of the stemless prostheses with six to eight strokes by an experienced surgeon.

Regarding the standard stems, the first stroke had always a lower force magnitude in comparison to the second one. The force magnitudes of the first strokes varied in the range from 2600 to 5945 N and did not show a difference between the head types. The mean values of the second stroke (maximum force) were slightly lower for eccentric CoCr28Mo6 with 5987 ± 592 N than for concentric Al_2O_3 heads with 8017 ± 204 N.

The stemless tapers were impacted with several strokes and their force magnitudes varied between 502 and 2938 N. There was no trend regarding the force magnitude sequence. Therefore, the maximum force occurred either at the first, sixth, or seventh hammer stroke with force magnitudes between 2063 and 2938 N.
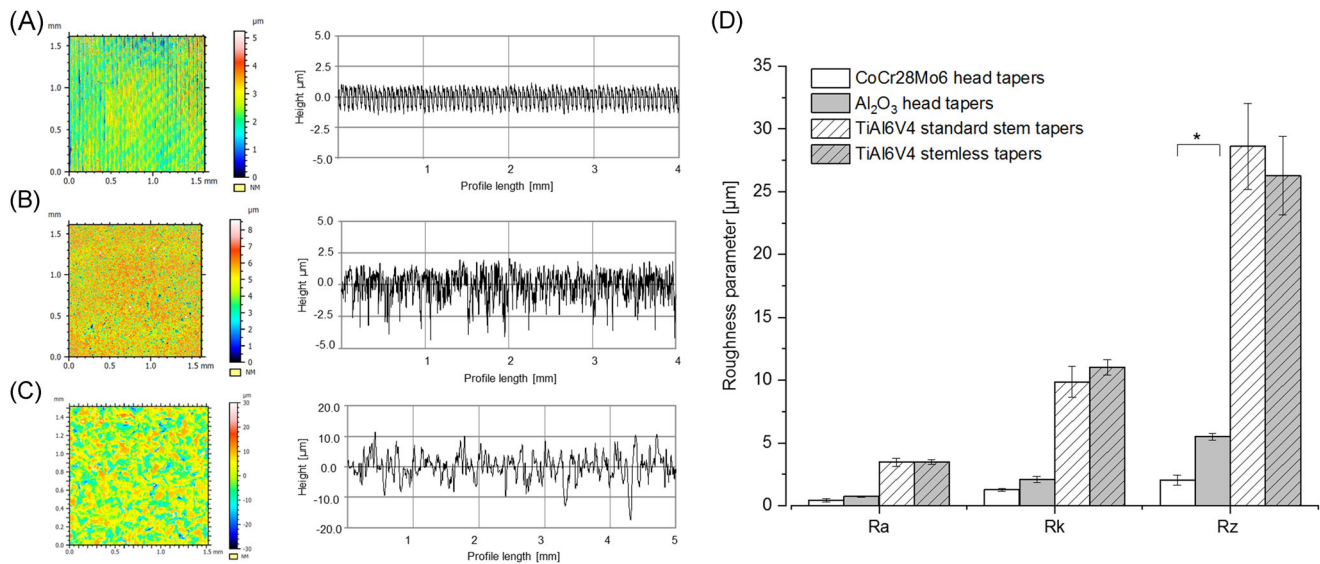
FIGURE 5 Confocal microscopic images, tactile roughness profiles, and roughness parameters of different taper surfaces. (A) CoCr28Mo6 alloy head taper, (B) Al_2O_3 ceramic head taper, and (C) TiAl6V4 alloy stem taper with corundum blasted surface. (D) Roughness parameters R_a, R_k, and R_z in μm for the tested head and stem tapers (mean ± standard deviation, one-way analysis of variance with Bonferroni post hoc test, R_z head tapers *$p = 0.014$, R_z stem tapers $p = 0.21$) [Color figure can be viewed at wileyonlinelibrary.com]

The maximum forces were significantly lower in the stemless impaction in Sawbones than for the standard stems in a stiff fixture, assembling the same concentric Al_2O_3 heads (mean force values of 2577–8017 N, respectively, $p = 0.004$).

The load–time history and impact duration for the maximum forces are illustrated in Figure 7. The standard stem assembly was characterized by presumably inertial peaks until the maximum force magnitude occurred. All tested stems showed this characteristic load–time relationship that was independent of the head material. The impact duration varied between 0.6 and 1.5 ms with a mean value of 1.25 ms. In contrast, the stemless impactions started with a steep increase in force and a following decrease of the maximum load. The loading duration was about 3 ms.

In addition, the vectors of the maximum resulting force of each hammer stroke were determined and their counterforces are illustrated in Figure 8A,B. The results show a marked difference between the two applied assembly strategies. Small directional deviations were present in the two-stroke impactions on standard stem tapers using the assembly device. The angular deviation to the ideal impaction direction varied between 3.3° and 6.2° for the Al_2O_3 heads and 4.3°–7.4° for the eccentric CoCr28Mo6 heads. No difference in angular deviation was observed between the first and the second hammer stroke in and between the different head groups (Figure 8C). For standard stems, the impact direction exhibited a pronounced shift in the x-direction with a mean force fraction of 8% than in the y-direction with only 3% on the resulting force (Figure 8D).

In contrast, the assembly of the stemless tapers into artificial bone revealed larger directional deviations between the multiple strokes with an angular deviation in the range of 18.9°–56.4° to the

ideal impaction direction. This directional variance was present in different stroke orders independent of the resulting force magnitude (Figure 8C). The directional shift in y-direction was greater than in x-direction with a mean share of 26% and 12%, respectively (Figure 8D).

3.3 | Pull-off forces

Afterward, the taper junctions were disassembled in pull-off tests to determine the taper strength. Force–displacement curves and force magnitudes of pull-off forces required to disassemble the test tapers are shown in Figure 9. Standard stems exhibit differences in force slope and maximal pull-off forces. The mean value of the pull-off force for the CoCr28Mo6 heads is about 3338.0 ± 349.4 N and for ceramic heads, about 3001.5 ± 672.5 N. For the first 250 μm of axial displacement, the eccentric CoCr28Mo6 head taper curves lie above the concentric Al_2O_3 head tapers. This indicates that the eccentric heads with TiAl6V4 stem taper require higher forces for similar micrometer displacement. With increasing axial displacement, the curves overlap and result in different maximal pull-off forces.

The ratio of the determined pull-off force against the maximal assembly force reveals that the eccentric CoCr28Mo6 head tapers exhibited a higher ratio than the concentric Al_2O_3 heads with mean values of 0.56 and 0.37, respectively (Figure 9B). Consequently, the same assembly force magnitudes require higher pull-off forces for the CoCr28Mo6/TiAl6V4 pairing than for the Al_2O_3/TiAl6V4 taper junctions. The stemless tapers could not be tested since the assembled samples were disrupted already during the cutting process of the fins.
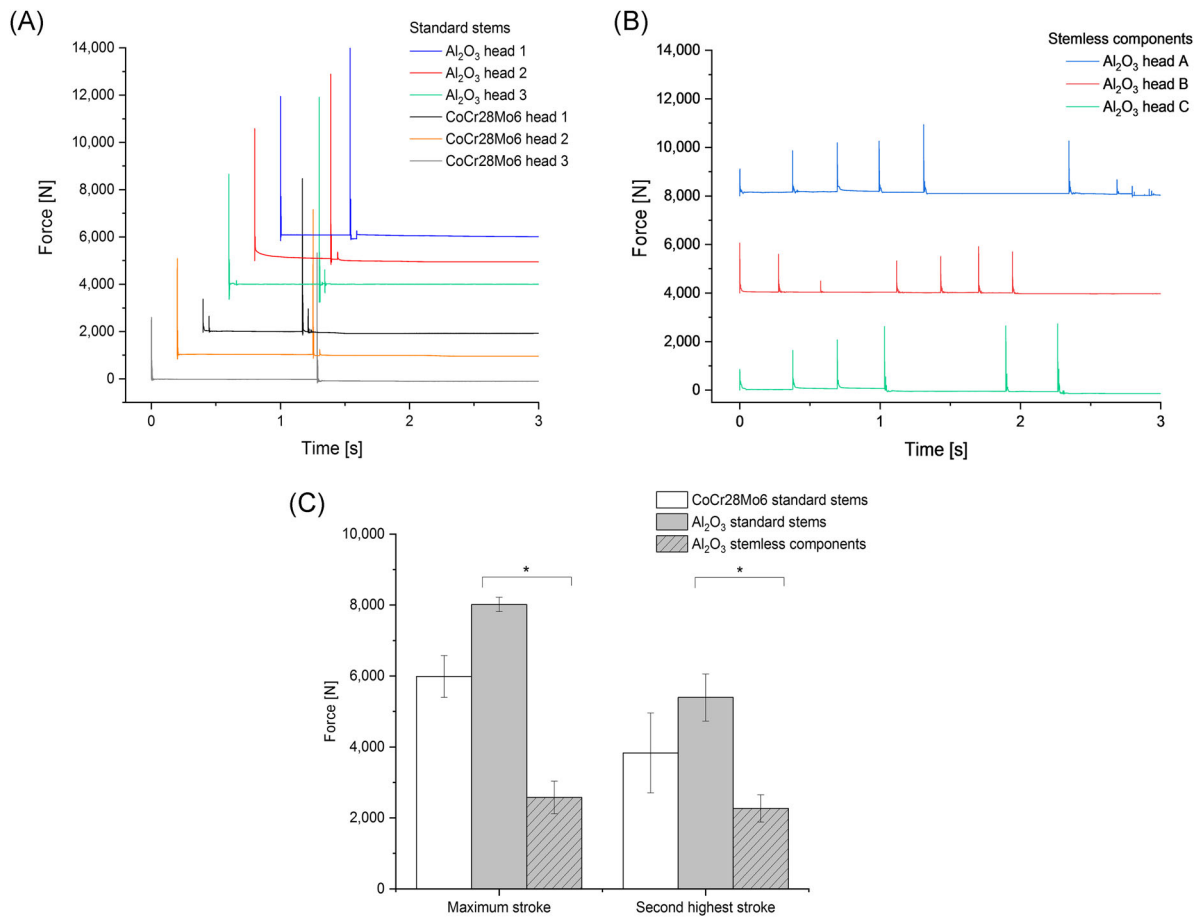
FIGURE 6 Impaction load–time curves for the tested implant groups measured with the sensorized impactor. (A) Load–time curves of the two-stroke impaction of standard stems with CoCr28Mo6 or Al_2O_3 humeral head (curves with offset: $x = 0.2$, $y = 1,000$). (B) Force signal of multiple stroke impaction of the stemless tapers with Al_2O_3 humeral heads in an artificial humeral bone (curves with offset: $y = 4000$). (C) Mean force magnitudes of the maximum loads and the second-highest impaction load for the tested taper combinations and design (mean ± standard deviation, one-way analysis of variance with Bonferroni post hoc test, maximum stroke on Al_2O_3 heads $*p = 0.004$, second-highest stroke on Al_2O_3 heads $*p = 2 \times 10^{-6}$) [Color figure can be viewed at wileyonlinelibrary.com]
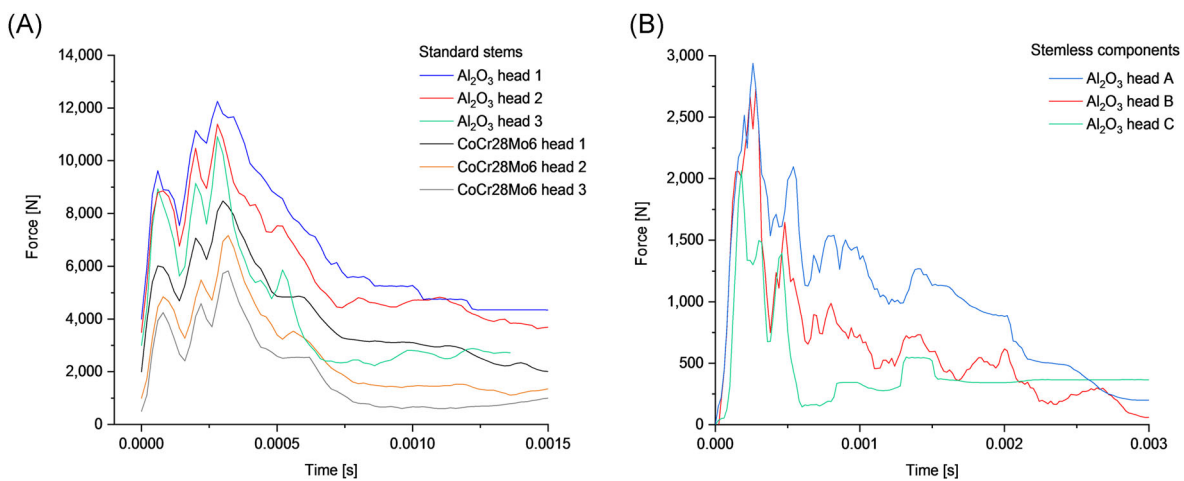

FIGURE 7 Load–time history of the maximum impaction forces for different study groups. (A) Load–time history of the impaction of humeral heads on standard stems (curves with offset: $y = 1000$). (B) Load–time curves for the impaction of stemless tapers with Al_2O_3 humeral heads [Color figure can be viewed at wileyonlinelibrary.com]
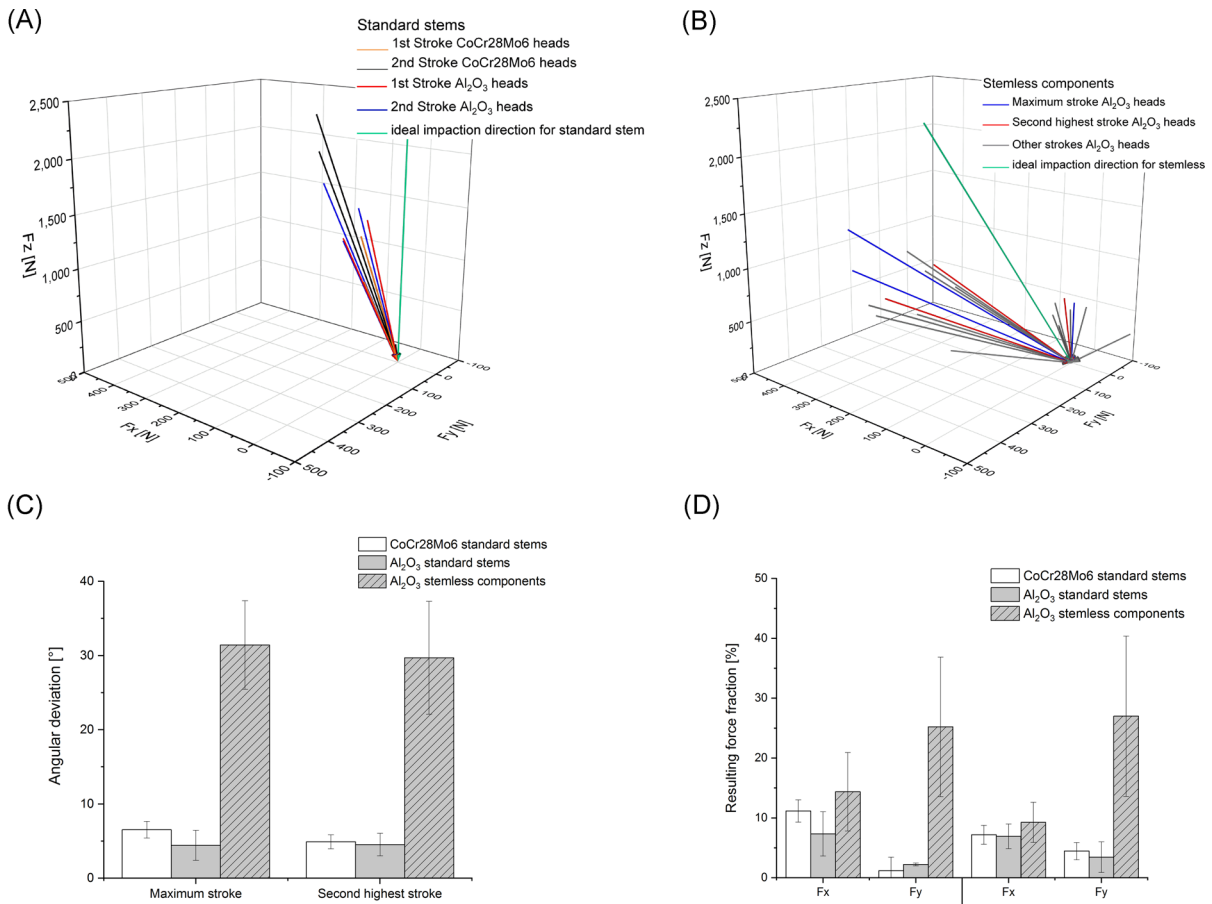
FIGURE 8 Counterforces of the maximum resulting force vectors for all hammer strokes detected in the three-dimensional force measuring platform. (A) Counterforce vectors of the strokes impacting standard stem tapers using the assembly device. (B) Counterforce vectors of multiple strokes impacting stemless tapers with the humeral heads in the artificial bone. (C) Angular deviation from the ideal impaction direction for the tested study groups. (D) Comparison of the F_x and F_y fractions (%) on the resulting maximum force for the strokes with the maximum and second-highest magnitude (mean ± standard deviation, one-way analysis of variance with Bonferroni post hoc test) [Color figure can be viewed at wileyonlinelibrary.com]
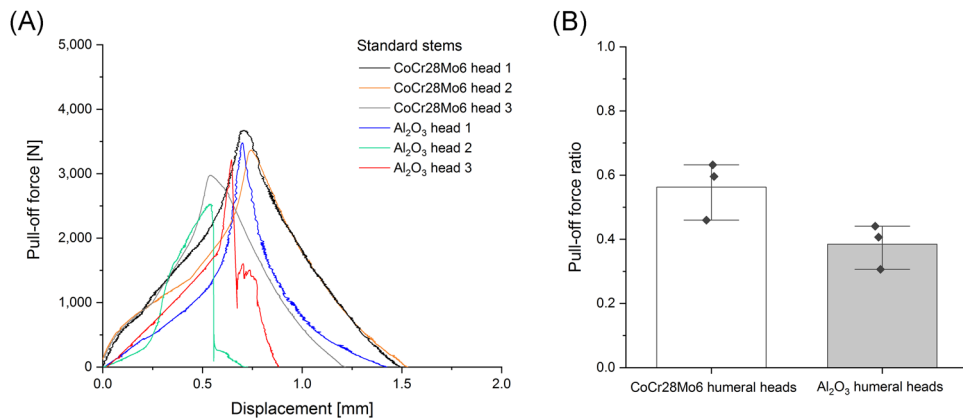

FIGURE 9 Results of the pull-off tests according to ASTM F2009 for standard stem tapers with eccentric CoCr28Mo6 or concentric Al_2O_3 or humeral heads. (A) Force–displacement curves of the tested implants. (B) The ratio between pull-off forces to maximum assembly force for the test samples of eccentric CoCr28Mo6 and concentric Al_2O_3 humeral heads (mean ± standard deviation, one-way analysis of variance with Bonferroni post hoc test, $p = 0.5$) [Color figure can be viewed at wileyonlinelibrary.com]

3.4 | Taper engagement area

Taper engagement areas were determined macroscopically on all head and stem tapers after disassembly and are shown in Figure 10 and Supporting Information Figure A. Exemplary photographs display a pronounced tilting of the CoCr28Mo6 humeral head in the distal direction to the taper axis. Corresponding local residues of the corundum blasted stem taper surface are evident in the CoCr28Mo6 head bore taper. Regarding the taper engagement area, concentric Al_2O_3 heads exhibit a smaller macroscopically deformed area in comparison to the eccentric CoCr28Mo6 heads (Figure 10A,B). The taper surfaces of the stemless components reveal no macroscopic clamping marks. However, an asymmetric distal taper engagement was observed in the Al_2O_3 bore tapers with few metallic residues in opposing areas that indicate a tilted assembly as demonstrated by the photographs in Figure 10B,C and Supporting Information Figure A.

4 | DISCUSSION

The aim of this study is to determine the effects of two common assembly techniques of anatomical shoulder endoprosthesis and to identify critical factors influencing taper strength. In particular, taper geometry and topography were characterized and force magnitude, impact direction, and taper engagement were determined.

Since the engagement mechanics between the aligned tapers affect the contact behavior, *taper geometry and roughness* were measured before testing. The head tapers exhibited a larger taper angle in comparison to the TiAl6V4 stem tapers. Similar taper angles have been described for contemporary hip tapers.[33,34] The resulting positive taper clearance of 0.05°–0.13° indicates that by axial alignment, a deeper (proximal) taper lock is envisaged. This is in line with the majority of hip tapers offered by different manufacturers that exhibit circumferential machining marks and an angular mismatch that leads to a proximal contact situation.[34] The very rough corundum blasted stem taper topography contributed to increased variations in the taper clearance in comparison to other taper designs (Figure 4).[34] On the basis of previous studies, the wide variation of taper clearance in the tested cohort should be considered critically since it plays a main role in taper strength and thereby influences the occurrence of micromotion.[19,20,35] In addition, increased angular mismatch have been described to promote component canting, and tilted taper fit was shown to generate high local stress concentrations for hip taper junctions.[21]

Different *impaction strategies* of the surgeon were observed for the tested assembly techniques. On the basis of surgical practice, standard stems were impacted with two strokes while placed in the assembly device in comparison with multiple strokes for the stemless tapers placed in the artificial bone. The magnitude of the applied forces varied between the different strokes. A progressive increase in force magnitude can be attributed to the taper's setting behavior that increases the reaction forces of subsequent strikes. Standard stems were impacted with significantly higher peak forces compared to stemless components. This difference may be attributed to variances in stiffness and damping behavior of the rigid assembly device in contrast to the brittle artificial bone. Furthermore, the surgeon limits consciously the impact forces to prevent any fracture damage to the bone. The large variability of the surgeon's impaction forces for similar implants and the same assembly procedure is in accordance with other impaction studies on modular hip implants.[26,36,37] To prevent micromotion and head loosening, forces of at least 4 kN are recommended for an adequate engagement length and sufficient taper strength of hip taper junctions.[29,38] In the case of the stemless shoulder impaction into the artificial bone, this requirement was not met. Furthermore, variances in mechanical properties between the tested artificial bone and human bone as well as in intraoperative patient position and incisional joint access influence the applied impact force and need to be further evaluated to make binding assembly force recommendations.
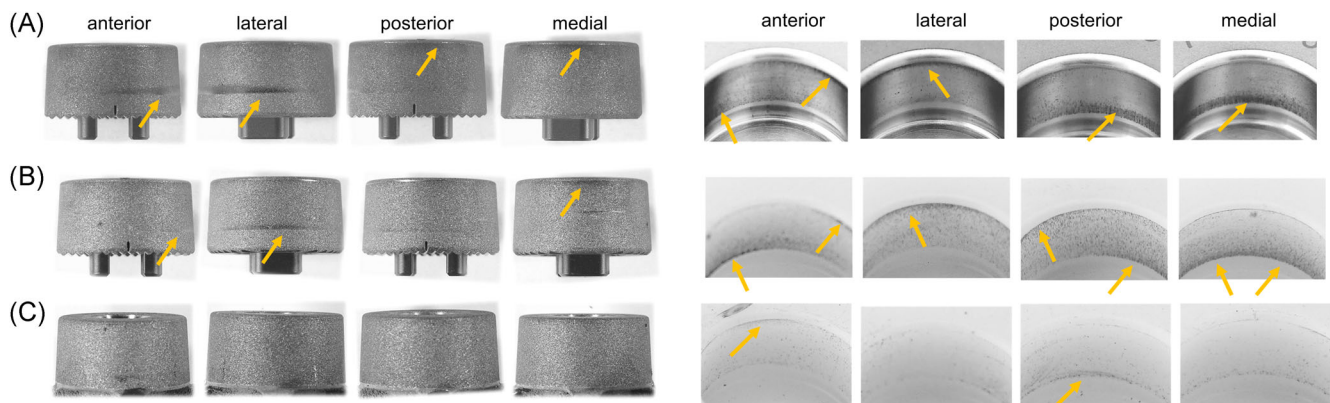

FIGURE 10 Photographs of exemplary taper surfaces according to the four radial sectors. Residual clamping marks can be seen on the stem taper and bore taper surface (orange arrow). (A) Standard stem taper that was assembled with an eccentric CoCr28Mo6 humeral head. (B) Standard stem taper that was aligned with a concentric Al_2O_3 humeral head. (C) Stemless taper and the corresponding concentric Al_2O_3 humeral head taper [Color figure can be viewed at wileyonlinelibrary.com]

The resulting taper strength for standard stems varied between eccentric CoCr28Mo6 and concentric Al_2O_3 heads with a mean ratio of 0.56 and 0.37, respectively. Rehmer et al.[38] and Pennock et al.[39] described that the taper strength was roughly equivalent to the magnitude of the strongest impaction. This finding was confirmed in the results using shoulder implants. Other studies have shown a linear correlation of increasing taper strength with assembly force, as well as the pull-off force to be around 45%–50% of the maximum impaction force.[29,37,38,40] These observations are again corroborated by the present results (Figure 9B). Studies showed that different material combinations exhibit similar turn-off forces but variances in turn-off moments. Due to the different elastic modulus, the highest turn-off moments were detected for Ti–Cr tapers followed by Ti–Ceramic taper combinations.[20,38] Since the tested femoral head groups did not only vary in material but also in eccentricity, taper angle, and profile height, these additional factors contribute to the observed difference in taper strength.

Impaction duration influences the setting behavior of the aligned components based on material relaxation. A previous finite element study assumed a linear loading history with an impaction duration of 2 s.[29] Nevertheless, the present results demonstrate that the time period of the dynamic assembly process is very short (<3 ms) and differs depending on the assembly procedure. Since the same impactor was used for both assembly procedures, the rigid assembly device generated a shorter impact duration, whereas the ductile artificial sponge bone allowed the force impulse to act longer (Figure 7). Krull et al.[41] demonstrate that the force–time characteristic of the applied impulse achieves different taper fixation and suggests maximizing impactor stiffness. On the basis of her work and the present findings, the use of an external assembly device is recommended to apply ideal impaction energy without damaging the patient's bone tissue. However, other intraoperative factors (e.g., an extension of the operating time, contamination risk) that can affect this decision must, therefore, be weighed. For direct bone impaction, the influence of bone stiffness on taper strength has to be investigated in future studies.

In addition, this study emphasizes the importance of an ideal axial *impaction direction*. Simulating intraoperative assembly conditions, the resulting force vector varied greatly from the ideal impact direction. Especially for stemless alignment, the angular deviation from ideal impact direction increased with each additional stroke (Supporting Information Figure B). The resulting force vector is influenced by additional factors, including the assembly setup, contact behavior between the tapers and implant-interfaces. However, the results highlight that the surgeon cannot guarantee an ideal axial effective force when using these assembly strategies. Frisch et al.[23,24] investigated the consequence of an off-axis impaction and found a significant deterioration of taper stability that might promote premature fretting motion. Furthermore, all tested taper junctions revealed an asymmetric taper engagement. The reasons for taper tilting are the present angular mismatch in combination with the variating effective force vectors. For the eccentric CoCr28Mo6 humeral heads, the pronounced lateral tilting was caused by the bending moment that occurred due to the lever arm between the stem axis and the head center point (Figure 11).

Tilted taper junctions are known to form crevices leading to a decreased contact area that enhances the risk of fretting and crevice corrosion.[42,43] Interfacial slip and micromotion due to cyclic implant loading continuously destroy the protective oxide layer of the passive metal alloys causing the release of wear particles and metal ions.[12,44] The formed crevice causes local oxygen depletion that accelerates the corrosion processes.[45,46] In this regard, the tested stem tapers were corundum blasted causing the incorporation of abrasive Al_2O_3 particles in the taper junctions.

There are some limitations to this study. The tested cohort comprises only two anatomical shoulder endoprosthesis types of one manufacturer and was limited in sample numbers. Consequently, the study results are restricted to the tested head geometry, materials, and stem types. Since the common assembly techniques were investigated, some of the variables, such as head material (ceramic, CoCr28Mo6 alloy) to eccentricity as well as implant design
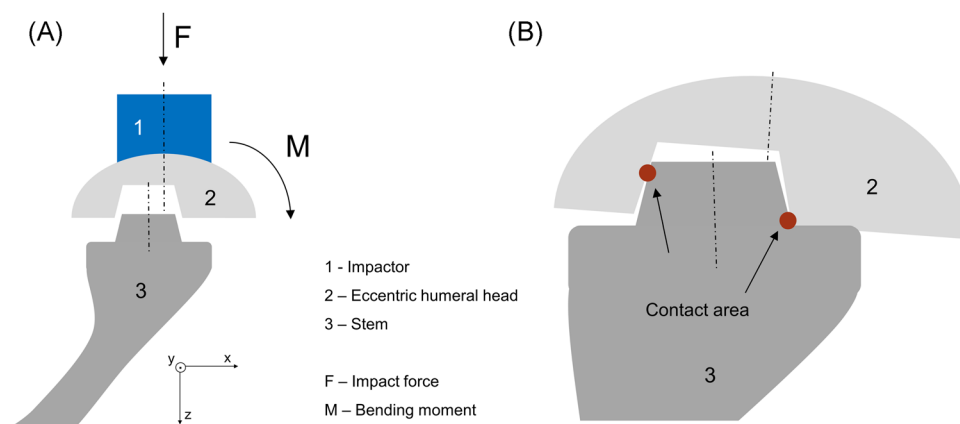

FIGURE 11 Scheme of the taper assembly of an eccentric humeral head on a stem taper using an impactor. (A) Bending moment leads to misalignment of the eccentric humeral head. (B) According to the bending moment, taper tilting occurs with canting in the lateral direction. 1—impactor; 2—eccentric humeral head; 3—stem. F, impact force; M, bending moment [Color figure can be viewed at wileyonlinelibrary.com]

(stemmed, stemless) to assembly strategy, could not be isolated. A precise focus on isolated variables is planned in a future study. In addition, the artificial bone does not ideally represent the mechanical properties of human bone. Thus, future studies should investigate typical force magnitudes impacting different implants in human cadaver bone. Furthermore, the impaction tests were performed by one shoulder surgeon and reflect his surgical experiences disregarding the subject variability. The assembled stemless tapers could not be tested regarding their taper strength since they disassembled prematurely during cutting preparation. Although there was no macroscopic evidence of a premature disruption of the taper lock for the stemmed tapers after stem shortening, an impact of the cutting process cannot be excluded. Further investigations are required to evaluate the influence of the cut-off grinding process. To derive the origin of taper tilting, in situ displacement measurements are suggested. This direct measurement would allow differentiating between an asymmetric seating during the component placement or a head canting during impaction. Future studies should consider direct displacement detection.

Nevertheless, this comprehensive study provides for the first time realistic impaction loads for ASA and reveals marked differences in assembly strategy. Stemless components that were directly impacted into artificial bone exhibited a significantly decreased peak load, leading to a deteriorated taper strength. In addition, taper tilting occurred independently of the applied assembly technique. Head eccentricity was identified as a critical promoting factor in taper tilting. On the basis of the present findings, the use of an external assembly device for stemmed shoulder implants is highly recommended to guarantee an axial impaction with a predefined impulse. A sensorized impactor is suggested for better intraoperative monitoring. For stemless shoulder endoprostheses, the in vivo application of a preassembled implant might be accompanied by resultant disadvantages (e.g., poor visibility during mounting).

5 | CONCLUSION

The assembly technique critically influences the impact load and consequently taper strength. We identified that the impact direction and head eccentricity are potential risk factors for taper malalignment.

AUTHOR CONTRIBUTIONS
Maria Herbster performed investigations, interpreted data, and drafted the manuscript. Alexander Berth performed the impaction tests and helped with the discussion and interpretation of data. Nicole Märtens helped with the study design and prepared the artificial bones. Marcel Robra developed the test setup, designed and manufactured the sensitized impactor. Florian Welzel provided the sensor and three-dimensional force measuring platform and supported with data interpretation. Frank Dallmann provided the samples and supported with technical data. Christoph H. Lohmann supervised the interpretation of the data and helped writing the manuscript. Thorsten Halle supervised the technical data and drafted the manuscript. Jessica Bertrand designed the study, helped writing the manuscript and to interpret the data. Joachim Döring helped with discussion and interpretation of data and supervised the project. We declare that all authors have read and approved the final submitted manuscript.

ORCID
Maria Herbster (iD) http://orcid.org/0000-0003-1385-7815

REFERENCES
1. Kim SH, Wise BL, Zhang Y, Szabo RM. Increasing incidence of shoulder arthroplasty in the United States. *J Bone Surg Am.* 2011;93: 2249-2254.
2. Oppermann J, Celik E, Bredow J, et al. Shoulder arthroplasty in Germany: 2005-2012. *Arch Orthop Trauma Surg.* 2016;136:723-729.
3. Heers G, Grifka J, An KN. Biomechanische Uberlegungen zur Schultergelenkendoprothetik. *Orthopade.* 2001;30:346-353.
4. Berth A, Pap G. Konzept und frühfunktionelle Ergebnisse eines neuen Doppelexzenter-Schulter-Prothesensystems. *Obere Extremität.* 2007; 2:73-80.
5. Irlenbusch U, End S, Kilic M. Differences in reconstruction of the anatomy with modern adjustable compared to second-generation shoulder prosthesis. *Int Orthop.* 2011;35:705-711.
6. Loew M. *AE-Manual der Endoprothetik*: Springer; 2010.
7. Upfill-Brown A, Satariano N, Feeley B. Stemless shoulder arthroplasty: review of short and medium-term results. *J Shoulder Elbow Surg.* 2019;3:154-161.
8. Schoch B, Werthel J-D, Schleck C, Sperling JW, Cofield RH. Does an increase in modularity improve the outcomes of total shoulder replacement? Comparison across design generations. *Int Orthop.* 2015; 39:2053-2060.
9. Boileau P, Moineau G, Morin-Salvo N, et al. Metal-backed glenoid implant with polyethylene insert is not a viable long-term therapeutic option. *J Shoulder Elbow Surg.* 2015;24:1534-1543.
10. Irlenbusch U, Blatter G, Gebhardt K, Pap G, Zenz P. Prospective study of double-eccentric hemi shoulder arthroplasty in different aetiologies: midterm results. *Int Orthop.* 2011;35:1015-1023.
11. Irlenbusch U, Rott O, Gebhardt K, Werner A. Rekonstruktion des Humeruskopfdrehpunktes in Abhängigkeit vom Prothesendesign. *Z Orthop Unfall.* 2008;146:211-217.

12. Arnholt CM, MacDonald DW, Malkani AL, et al. Corrosion damage and wear mechanisms in long-term retrieved CoCr femoral components for total knee arthroplasty. *J Arthroplasty*. 2016;31:2900-2906.

13. Hallab NJ, Messina C, Skipor A, Jacobs JJ. Differences in the fretting corrosion of metal–metal and ceramic–metal modular junctions of total hip replacements. *J Orthop Res*. 2004;22:250-259.

14. Willert HG, Semlitsch M. Reactions of the articular capsule to wear products of artificial joint prostheses. *J Biomed Mater Res*. 1977;11:157-164.

15. Crackau M, Märtens N, Harnisch K, et al. In vivo corrosion and damages in modular shoulder prostheses. *J Biomed Mater Res*. 2020;108:1764-1778.

16. Day JS, MacDonald DW, Abboud JA, et al. Mechanically assisted crevice corrosion damage in shoulder arthroplasty is comparable to hip arthroplasty. In: Greenwald AS, Kurtz SM, Lemons JE, Mihalko WM, eds. *Modularity and Tapers in Total Joint Replacement Devices*. ASTM International; 2015:181-191.

17. Teeter MG, Carroll MJ, Walch G, Athwal GS. Tribocorrosion in shoulder arthroplasty humeral component retrievals. *J Shoulder Elbow Surg*. 2016;25:311-315.

18. Mali SA, Gilbert JL. *New test protocol to correlate micromotions and fretting corrosion in modular tapers*. Society for Biomaterials; 2014.

19. Donaldson FE, Coburn JC, Siegel KL. Total hip arthroplasty head-neck contact mechanics. A stochastic investigation of key parameters. *J Biomech*. 2014;47:1634-1641.

20. Fallahnezhad K, Farhoudi H, Oskouei RH, Taylor M. Influence of geometry and materials on the axial and torsional strength of the head-neck taper junction in modular hip replacements. A finite element study. *J Mech Behav Biomed Mater*. 2016;60:118-126.

21. Buente D, Bryant M, Ward M, Neville A, Morlock M, Huber G. The taper corrosion pattern observed for one bi-modular stem design is related to geometry-determined taper mechanics. *Med Eng Phys*. 2017;46:79-88.

22. Lemons JE. Studies of modular connections for surgical implant devices. In: Greenwald AS, Kurtz SM, Lemons JE, Mihalko WM, eds. *Modularity and Tapers in Total Joint Replacement Devices*. ASTM International; 2015:379-395.

23. Frisch NB, Lynch JR, Banglmaier RF, Silverton CD. The Effect of Impact Location on Force Transmission to the Modular Junctions of Dual-Taper Modular Hip Implants. *J Arthroplasty*. 2016;31:2053-2057.

24. Frisch NB, Lynch JR, Banglmaier RF, Silverton CD. The stability of dual-taper modular hip implants: a biomechanical analysis examining the effect of impact location on component stability. *Arthroplast Today*. 2017;3:119-124.

25. Nambu S, Obert R, Roark M, et al. Accelerated fretting corrosion testing of modular necks for total hip arthroplasty. In: Greenwald AS, Kurtz SM, Lemons JE, Mihalko WM, eds. *Modularity and Tapers in Total Joint Replacement Devices*. ASTM International; 2015:237-258.

26. Heiney JP, Battula S, Vrabec GA, et al. Impact magnitudes applied by surgeons and their importance when applying the femoral head onto the Morse taper for total hip arthroplasty. *Arch Orthop Trauma Surg*. 2009;129:793-796.

27. Mroczkowski ML, Hertzler JS, Humphrey SM, Johnson T, Blanchard CR. Effect of impact assembly on the fretting corrosion of modular hip tapers. *J Orthop Res*. 2006;24:271-279.

28. Panagiotidou A, Cobb T, Meswania J, et al. Effect of impact assembly on the interface deformation and fretting corrosion of modular hip tapers. An in vitro study. *J Orthop Res. Jan*. 2018;36(1):405-416.

29. English R, Ashkanfar A, Rothwell G. The effect of different assembly loads on taper junction fretting wear in total hip replacements. *Tribol Int*. 2016;95:199-210.

30. Mathys Ltd. *Surgical technique Affinis short. Short stem total shoulder prosthesis*; 2017.

31. ASTM. *F2009 test method for determining the axial disassembly force of taper connections of modular prostheses*. West Conshohocken, PA: ASTM International; p. 4.

32. Haynes W. Bonferroni correction. In: Dubitzky W, Wolkenhauer O, Cho K-H, Yokota H, eds. *Encyclopedia of Systems Biology*. Springer; 2013:154.

33. Bechstedt M, Gustafson JA, Mell SP, et al. Contact conditions for total hip head-neck modular taper junctions with microgrooved stem tapers. *J Biomech*. 2020;103:109689.

34. Mueller U, Braun S, Schroeder S, Sonntag R, Kretzer JP. Same same but different? 12/14 stem and head tapers in total hip arthroplasty. *J Arthroplasty*. 2017;32:3191-3199.

35. Chana R, Esposito C, Campbell PA, Walter WK, Walter WL. Mixing and matching causing taper wear: corrosion associated with pseudotumour formation. *J Bone Joint Surg Br*. 2012;94:281-286.

36. Nassutt R, Mollenhauer I, Klingbeil K, Hennig O, Grundei H. Relevance of the insertion force for the taper lock reliability of a hip stem and a ceramic femoral head. *Biomed Tech*. 2006;51:103-109.

37. Scholl L, Schmidig G, Faizan A, TenHuisen K, Nevelos J. Evaluation of surgical impaction technique and how it affects locking strength of the head-stem taper junction. *Proc Inst Mech Eng H*. 2016;230:661-667.

38. Rehmer A, Bishop NE, Morlock MM. Influence of assembly procedure and material combination on the strength of the taper connection at the head-neck junction of modular hip endoprostheses. *Clin Biomech*. 2012;27:77-83.

39. Pennock AT, Schmidt AH, Bourgeault CA. Morse-type tapers. *J Arthroplasty*. 2002;17:773-778.

40. Danoff JR, Longaray J, Rajaravivarma R, Gopalakrishnan A, Chen AF, Hozack WJ. Impaction force influences taper-trunnion stability in total hip arthroplasty. *J Arthroplasty*. 2018;33:S270-S274.

41. Krull A, Morlock MM, Bishop NE. Maximizing the fixation strength of modular components by impaction without tissue damage. *Bone Jt Res*. 2018;7:196-204.

42. Hussenbocus S, Kosuge D, Solomon LB, Howie DW, Oskouei RH. Head-neck taper corrosion in hip arthroplasty. *BioMed Res Int*. 2015;2015:758123.

43. Panagiotidou A, Meswania J, Hua J, Muirhead-Allwood S, Hart A, Blunn G. Enhanced wear and corrosion in modular tapers in total hip replacement is associated with the contact area and surface topography. *J Orthop Res*. 2013;31:2032-2039.

44. Balachandran S, Zachariah Z, Fischer A, et al. Atomic scale origin of metal ion release from hip implant taper junctions. *Adv Sci*. 2020;7:1903008.

45. Brown SA, Flemming CAC, Kawalec JS, et al. Fretting corrosion accelerates crevice corrosion of modular hip tapers. *J Appl Biomater*. 1995;6:19-26.

46. John Cooper H, Della Valle CJ, Berger RA, et al. Corrosion at the head-neck taper as a cause for adverse local tissue reactions after total hip arthroplasty. *J Bone Joint Surg Am*. 2012;94:1655-1661.

SUPPORTING INFORMATION

Additional Supporting Information may be found online in the supporting information tab for this article.